Journal of Materials Chemistry B

ROYAL SOCIETY OF CHEMISTRY

PAPER

View Article Online
View Journal | View Issue

Cite this: *J. Mater. Chem. B*, 2026, **14**, 1882

Visualisation of adjuvant penetration into plant waxes by fluorescence of Nile Red

Petr S. Sherin, *[a] Michelle Wong Chap Lan, [a] Nicholas J. Brooks, [a] Markus Rueckel*[b] and Marina K. Kuimova *[a]

Received 16th September 2025,
Accepted 10th January 2026

DOI: 10.1039/d5tb02086g

rsc.li/materials-b

Epicuticular wax is the outermost layer of plant leaves, whose function is to protect the leaf, including preventing uncontrolled water loss. However, the resilience of this layer may present challenges in agriculture by preventing the ingress of pesticides and herbicides. Chemical formulations used in modern agrochemistry to enhance the efficiency of pesticides and herbicides often contain softening adjuvants that are expected to facilitate the permeability of waxes to chemicals. However, the mechanism of the adjuvants' action is relatively unexplored. Here, we report that an environmentally sensitive fluorophore, **Nile Red** (NR), can be used to directly visualise the penetration of adjuvants inside common plant waxes, such as Carnauba and Candelilla. In particular, we utilised Fluorescence Lifetime Imaging Microscopy (FLIM), which revealed that NR's emission is quenched by wax components. However, the penetration of adjuvants of different chemical structures significantly reduced the quenching, leading to an increase in NR's fluorescence intensity and lifetime. This effect allows the direct visualisation and kinetic monitoring of penetration of agrochemicals within the semicrystalline plant waxes using conventional fluorescent microscopes and opens a new area for the application of NR.

Introduction

Epicuticular wax is the outermost layer of plant leaves, protecting them from desiccation and alleviating damage by UV radiation and mechanical abrasion.[1] Controlling permeability through this layer is important for modern agriculture to deliver active ingredients inside the leaf efficiently. Currently, this control relies on the use of complex formulations, which include adjuvants that are expected to soften the wax layer and thus facilitate the permeation of various chemicals, such as pesticides and herbicides. Despite the wide use of adjuvants in agriculture, their action mechanisms and the changes they cause in the structural and dynamic properties of plant waxes are largely unknown, thus precluding rational strategies for their design.

Carnauba wax, from Brasilian palm tree, *Copernicia prunifera*, is one of the most characterised natural waxes[2] and widely used in a variety of model systems.[3] This wax is a complex mixture of long-chain esters and alcohols (more than 80% of wax content), including fatty acids, hydrocarbons, diols and other compounds.[2,3] Carnauba wax is not a uniform solid; it contains microcrystalline regions embedded in an amorphous matrix.[4] The chemical compositions of both phases are currently still unknown. The presence of orthorhombic unit cells[5,6] evidences the formation of a crystalline phase, which is presumably formed by long, linear and saturated chains. These efficiently packed domains have a high melting temperature (80–86 °C), are brittle in nature and provide the hardness to the Carnauba wax.[2,3,6] The amorphous phase is significantly less ordered[5–7] and grants the flexibility to the wax.[3] The crystalline network melts and reversibly recrystallises,[4,5] which suggests the carnauba wax as a phase-change material.[8] The ratio between crystalline and amorphous phases varies significantly from species to species.[2]

Recently, we suggested a novel microscopy method to visualise the crystalline and amorphous phases of Carnauba plant wax and to quantify the changes in viscosity within these phases upon water and adjuvant penetration.[9] This method was based on the application of 'molecular rotors', synthetic fluorophores, whose intensity and lifetime are sensitive to the microviscosity of their environment. Our results have shown that water penetration mainly softens the crystalline phase, while the adjuvant largely decreases the viscosity within the amorphous phase of Carnauba wax.

Here, we set out to study the impact of commercial adjuvants on the structure and properties of plant waxes by using fluorescence microscopy combined with an environmentally sensitive, commercially available dye, **Nile Red** (NR, see Chart 1 for chemical structure). NR is a well-known charge-transfer dye

[a] *Chemistry Department, Imperial College London, 82 Wood Lane, W12 0BZ, London, UK. E-mail: p.sherin@imperial.ac.uk, m.kuimova@imperial.ac.uk*
[b] *BASF SE, Carl-Bosch-Strasse 38, Ludwigshafen am Rhein, 67056, Germany. E-mail: markus.rueckel@basf.com*

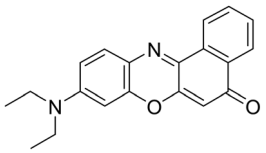

Nile Red

Chart 1 Chemical structure of **Nile Red** (NR).

with a large dipole moment in the excited state. NR shows a strong shift in the maximum of its fluorescence spectrum in response to the changes in polarity of its local environment.[10–14] Recent studies have shown that NR's lifetime is sensitive to hydration and ordering within lipid bilayers and cellular plasma membranes,[15–18] and could be used for the identification of microplastic particles,[19] characterisation of ionic liquids[20] and to monitor drug penetration into the skin.[21] Our rationale was that a penetration of adjuvants would likely change the polarity of the wax, leading to marked shifts in NR's fluorescence spectrum, allowing facile monitoring. However, opposite to these expectations, we discovered that the permeation of adjuvants did not significantly change the spectral response of NR in the wax but instead resulted in a large increase in the fluorescence intensity and lifetime of NR. Here, we investigate the mechanism behind this effect and utilise microscopy monitoring to detect the disruption of wax structure by various agriculturally relevant chemicals (adjuvants and emulsifiers).

Materials and methods

Materials

Nile Red (product number N3013) and Carnauba Wax (product number 243213) from Sigma Aldrich, Candelilla Wax from SoapKitchen, (product number TSK-BUT002, UK), emulsifier (Agnique® CSO40, purity >99.5%) and softening adjuvants (Plurafac® LF431, Plurafac® LF1300, Agnique® SBO10, Lutensol® XP80, all with purity >99.5%) from BASF, were used as received. The syntheses of BODIPY-based molecular rotors B10[22] and B6++[23] were reported previously. All organic solvents used in this work (*n*-pentane, toluene, castor oil, chloroform, acetonitrile and methanol) were spectroscopic grade from Sigma Aldrich; cholesterol (CL), egg yolk sphingomyelin (SM) and distearoylphosphatidylcholine (DSPC) were obtained from Avanti Polar lipids as dry powder (CL) or chloroform solutions (SM and DSPC). To simulate agricultural conditions, tap water was used in all experiments.

Absorption and fluorescence spectra, fluorescence lifetime measurements

Rectangular quartz cuvettes (10 × 10 mm^2, total volume 3.5 mL, catalogue number 3-Q-10-GL14-S from Starna, UK) were used for all spectroscopic measurements. Absorption and fluorescence spectra were recorded using an Agilent 8453 UV-vis spectrophotometer and a Fluoromax-4 spectrofluorometer (Jobin-Yvon, Horiba), respectively. All liquid samples had an absorbance below 0.15 at the absorption maxima. All fluorescence spectra were corrected for wavelength-dependent sensitivity of detection.

Time-resolved fluorescence decays were measured using a DeltaFlex setup (Jobin-Yvon, Horiba) operating *via* Time Correlated Single-Photon Counting (TCSPC). The excitation source was 467 nm NanoLEDs (Horiba, FWHM <200 ps); the detection wavelength and spectral width were selected with the in-built monochromator as indicated. The fluorescence decays were recorded until 10 000 counts at the maximum and 100 ns time window with 4096-time bins. Fluorescence decays were fitted individually or globally using a sum exponential decay function (details are specified in the text). The resulting goodness-of-fit parameter χ^2 was between 1.0 and 1.3. The instrument response function (IRF) was measured using a dilute Ludox solution at the excitation wavelength.

Lipid staining with NR

Stock solutions of lipids were prepared by dissolution (CL) or dilution (SM, DSPC) with chloroform to concentrations of 50 mg mL^{-1} for CL and 25 mg mL^{-1} for SM and DSPC. Small aliquots (0.35 μL) of NR stock solutions (3 mM in chloroform) were added to small volumes of stock solutions containing 1 mg of lipids; the binary mixtures of lipids (CL/SM and CL/DSPC) were prepared with the ratio of 1/1 w/w and the total weight of lipids of 1 mg. The mixtures were deposited on coverslips (1.0 class borosilicate glass, 22 × 50 mm, VWR International, Germany) and dried in air. All samples were placed in a desiccator overnight to remove any residual chloroform.

Wax staining with NR

Solid wax powder (10 mg) and chloroform (80 μL) were placed in a glass vial. Aliquots of NR stock solutions (3.5 μL of 3 mM in chloroform) were added to the wax in chloroform, to make up 330 ppm to the dry wax weight. These glass vials were heated up to 70 °C with a digital heater (model No 949303, VWR International, USA) to achieve complete melting of the wax until it formed a homogenous solution. Then the hot mixtures were deposited onto pre-heated (75 °C) coverslips (1.0 class borosilicate glass, 22 × 50 mm, VWR International, Germany). Fast evaporation of chloroform provided a quick and even distribution of the wax over the coverslip with a thickness variation in the range of 12–20 μm. The samples of wax on coverslips were slowly cooled down on the heating plate (MR Hei-Standard, Heidolph, Germany) at the rate of 20 °C/15 min and used in microscopy experiments.

Exposure of wax to aqueous solutions and neat adjuvant

The long-term exposure of wax to aqueous solutions required the retention of this solution on top of the wax without evaporation. Thus, a well was formed around the wax with a volume of 200–500 μL. For this purpose, we used plastic grids from 8-well chambered microscope slides (Lab-Tek Nunc II, part number 155411, ThermoFisher Scientific, Germany). The plastic grid, obtained after the removal of the coverslip from

the chamber, was placed over the melted wax before the samples were completely cooled and gently pressed to remove the wax from underneath all plastic edges. After the slow cooling of wax samples was completed, the plastic grid was fixed on the coverslip with Superglue to prevent grid displacement and water leakages during experiments. Aliquots of 300 μL of tap water in the absence or presence of 1000 ppm of emulsifier or adjuvant were added to individual wells. The whole plastic grid was covered by a coverslip to prevent water evaporation. The confocal and FLIM images were recorded at different time intervals after the wax exposure to aqueous solutions.

Neat adjuvants were placed as small drops (1 μL) onto the wax surface and left overnight at ambient lab conditions for adjuvants' dissolution within the wax.

Confocal fluorescence imaging

NR-stained wax samples (500 ppm NR) were imaged using an inverted confocal laser-scanning microscope, Leica TCS SP8 (Leica Microsystem Ltd, Germany). 400 μL of 1000 ppm Plurafac® LF431, dissolved in hard water, was applied to the wax layer. The fluorescence intensity changes of NR were imaged over time, roughly in the middle of the wax layer, using an excitation wavelength of 514 nm and a detection band 610–700 nm.

Multiphoton fluorescence imaging

Multiphoton fluorescence imaging of wax samples stained with NR was performed using an inverted confocal laser-scanning microscope, Leica TCS SP5 II (Leica Microsystem Ltd, Germany). Room temperature imaging was carried out with x63 (N.A. 1.2) HCX PL APO CS water immersion objective lens with a correction collar (11506279, Leica Microsystem Ltd, Germany). All fluorescent dyes were excited at 930 nm with a Ti: Sapphire pulsed laser source (680–1080 nm, 80 MHz, 140 fs, Chameleon Vision II, Coherent Inc., Germany) and the emission intensity was recorded at 540–700 nm. All images were processed in the Leica Application Suite X (LAS X, v. 3.7.1) software package.

Spectrally resolved fluorescence imaging

Spectrally resolved images were recoded using a λ-scan of Leica SP5 II microscope with 20 nm detection band and 10 nm step over the range of 480–740 nm following the multiphoton excitation at 930 nm. The emission spectra were generated by LAS and exported for further processing.

Fluorescence lifetime imaging microscopy (FLIM)

FLIM images of 256 × 256 pixels were obtained using the same Leica TCS SP5 II microscope with x63 objective coupled with a TCSPC module SPC830 (Becker&Hickl, Germany) and internal FLIM detector PMH-100 (Becker&Hickl, Germany), synchronised to the Ti: Sapphire pulsed laser, using the same excitation and detection as for multiphoton imaging. The laser power was maintained at <80 mW before entering the microscope to avoid photodamage (<0.3 μW on the sample). FLIM data were acquired in the range 540–700 nm with time intervals varying in the range of 60–180 seconds per frame, depending on the emission intensity from a sample. *z*-Stacks of FLIM data were recorded at different distances from the bottom ($z = 0$ μm) to the top of the wax layer (*ca.* 12–20 μm, depending on wax thickness) with a step size of 3–4 μm.

FLIM data were analysed using the SPCImage v.8.5 software (Becker & Hickl, Germany) with an incomplete exponential decay model with offset values fixed to zero. The Maximum Likelihood Entropy (MLE) fitting algorithm was used, particularly suitable for low-intensity signals.[24] The binning of pixels (rectangular bin 1, 3 × 3 pixels) was used for all data to produce a typical peak count in the decay maximum in the range of 100–200 counts per pixel (which is deemed sufficient for the MLE analysis); thresholding was adjusted from sample to sample to remove pixels of low intensity from the analysis. All decays were fitted using a bi-exponential decay function with $1.0 < \chi^2 < 1.3$. A pseudo-colour scale was assigned to each fluorescence lifetime, amplitude and the goodness of fit (χ^2) values (red for small values and blue for large values) to provide corresponding maps. The lifetime values and errors presented in the text are mean values and standard deviations calculated from histograms corresponding to one FLIM data frame (total amount of pixels in the range of 40 000–65 536). The reproducibility of the data was confirmed in at least two independent experiments, with at least three frames collected per condition.

Results and discussion

Changes in NR intensity upon adjuvant penetration within the wax

We initially used Carnauba wax as a model system for plant wax, a widely accepted and readily available model.[2,3] Recently, we used BODIPY-based molecular rotors to monitor the softening of the amorphous phase of Carnauba wax upon exposure to aqueous adjuvant Plurafac® LF431.[9] Thus, a sample of Carnauba wax, stained with 500 ppm of NR, was exposed to the aqueous solution containing 1000 ppm of Plurafac® LF431. Within one hour, we observed a substantial increase in the overall NR fluorescence from the wax, which we assigned to the penetration of adjuvant, based on the timescales seen in our previous experiments, where adjuvant penetration under identical conditions was monitored using molecular rotors.[2,9] We also detected the formation of net-like structures with bright fluorescence intensity (Fig. 1).

To clarify the localisation of NR within the wax, we prepared Carnauba wax samples stained simultaneously with NR and a BODIPY-based molecular rotors B10 or B6++ (chemical structures are shown in Chart S1 of SI). Our previous work showed that these dyes selectively stain amorphous and crystalline phases of Carnauba wax, respectively.[9] Patterns, visualised by NR, colocalise with amorphous phase-located B10 (Fig. 2(a1–c1)), and they do not coincide with crystalline phase-located B6++ (Fig. 2(a2–c2)); details on quantitative analysis are given in the SI, including plots of intensities in two channels (Fig. S1). This

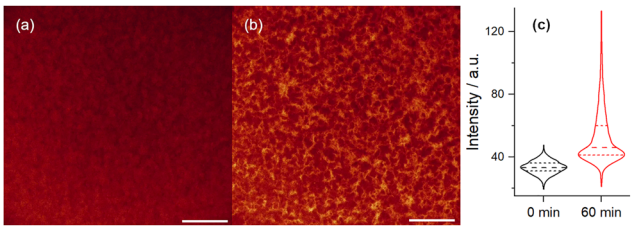

Fig. 1 Fluorescence intensity images obtained with Carnauba wax sample, stained with 500 ppm of NR, at (a) 0 min and (b) 60 min of exposure to the aqueous solution containing 1000 ppm of Plurafac® LF431. (c) Intensity distributions in (a) and (b); dashed lines represent median values, and short dashed lines 25–75% of pixels. Excitation at 514 nm and detection at 610–700 nm; scale bars are 50 μm.

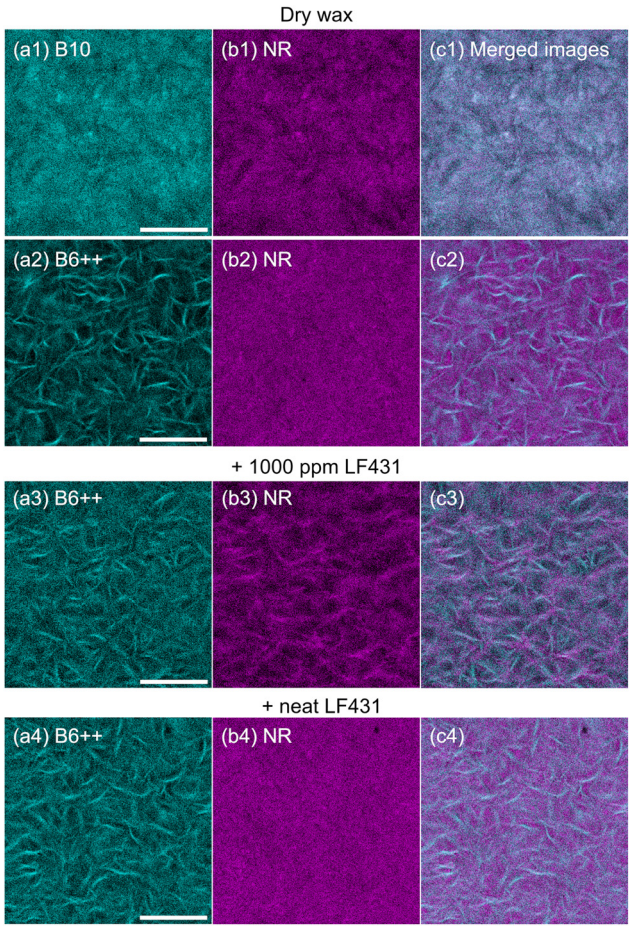

Fig. 2 Fluorescence intensity images recorded for Carnauba wax samples co-stained with 30 ppm of **Nile Red** (magenta) and 100 ppm of B10 or B6++ (cyan), the latter visualising the amorphous and crystalline phases of wax, respectively. (a1–c2) Dry wax; (a3–c3) exposed for 3 hours to the aqueous solution of 1000 ppm of Plurafac® LF431; (a4–c4) exposed to the neat Plurafac® LF431. Excitation at 930 nm and detection at 480–530 nm for B10 and B6++ (a1–a4) and 600–700 nm for NR (b1–b4); the merged images are shown in (c1–c4). Scale bars are 20 μm.

confirms that NR is localised within the amorphous phase of Carnauba wax, both before and after adjuvant staining (Fig. 2(a3–c3 and a4–c4)).

Changes in NR emission spectra and lifetime upon adjuvant penetration within the wax

Significant changes in NR fluorescence (Fig. 1) indicate substantial changes in the environment surrounding the dye. As NR is known to be a polarity-sensitive dye, we initially hypothesised that these changes were due to changes in the polarity of the wax upon adjuvant penetration. Thus, we used spectrally resolved fluorescence imaging following multiphoton excitation of NR in the wax. Multiphoton excitation was necessary due to significant scattering observed in these turbid and thick samples, as seen previously.[9] We recorded fluorescence spectra from Carnauba wax samples containing 330 ppm of NR and exposed to (i) the aqueous solution (1000 ppm) and (ii) the neat adjuvant of Plurafac® LF431.

NR within the amorphous wax phase emits with a maximum at 600 nm (Fig. 3c), which is typical for low-polarity solvents such as chloroform.[13] Importantly, the spectral maximum shows a minor shift upon addition of dilute or even neat adjuvant solutions to the wax (1–2 nm for the aqueous solution and approx. 10 nm for the neat compound, Fig. 3c). Since spectral shifts of NR are known to respond to polarity,[11–14,17] we conclude that the addition of the adjuvant does not significantly change the polarity of the environment or the localisation of NR within the wax.

However, the intensity of NR emission increases significantly upon penetration of the adjuvant (Fig. 1). To understand this unexpected result, we recorded Fluorescence Lifetime Imaging Microscopy (FLIM) data for the dry wax. Fluorescence decays of NR emission within the wax, recorded with FLIM over the whole emission band 540–700 nm, are best fitted with biexponential functions (Fig. S2). NR is a charge-transfer (or push–pull) dye which exhibits solvatochromic behaviour, *i.e.* wavelength-dependent decays.[11–14] However, only minor changes in NR fluorescence decays were observed between 540–700 nm (recorded with a 20 nm step, Fig. S3). Therefore, in the absence of a visible solvatochromic behaviour, the two decay components are related to two different environments of NR within the amorphous phase of the wax. For simplicity of data representation, we used the intensity-weighted lifetime (τ_i).

Further, we investigated the impact of NR concentration on its spectral and photophysical properties. NR exhibits minor changes in the shape of its emission spectrum, as well as a significant shortening of both lifetime components with increasing concentration (Fig. S4). The latter is consistent with the aggregation of NR within the wax at concentrations above 500 ppm. Thus, all further experiments were carried out at dye concentrations below 350 ppm to minimise aggregation effects while keeping an intense signal for fast acquisition of FLIM data.

Finally, we verified a possible impact of chloroform and residual quantities of hydrochloric acid formed from chloroform degradation on the photophysics of NR within the wax (Fig. S5 and corresponding comment in the SI). Samples of NR-containing waxes were prepared using four methods: *via* the dissolution in (i) chloroform and (ii) toluene, as well as (iii and iv), where the

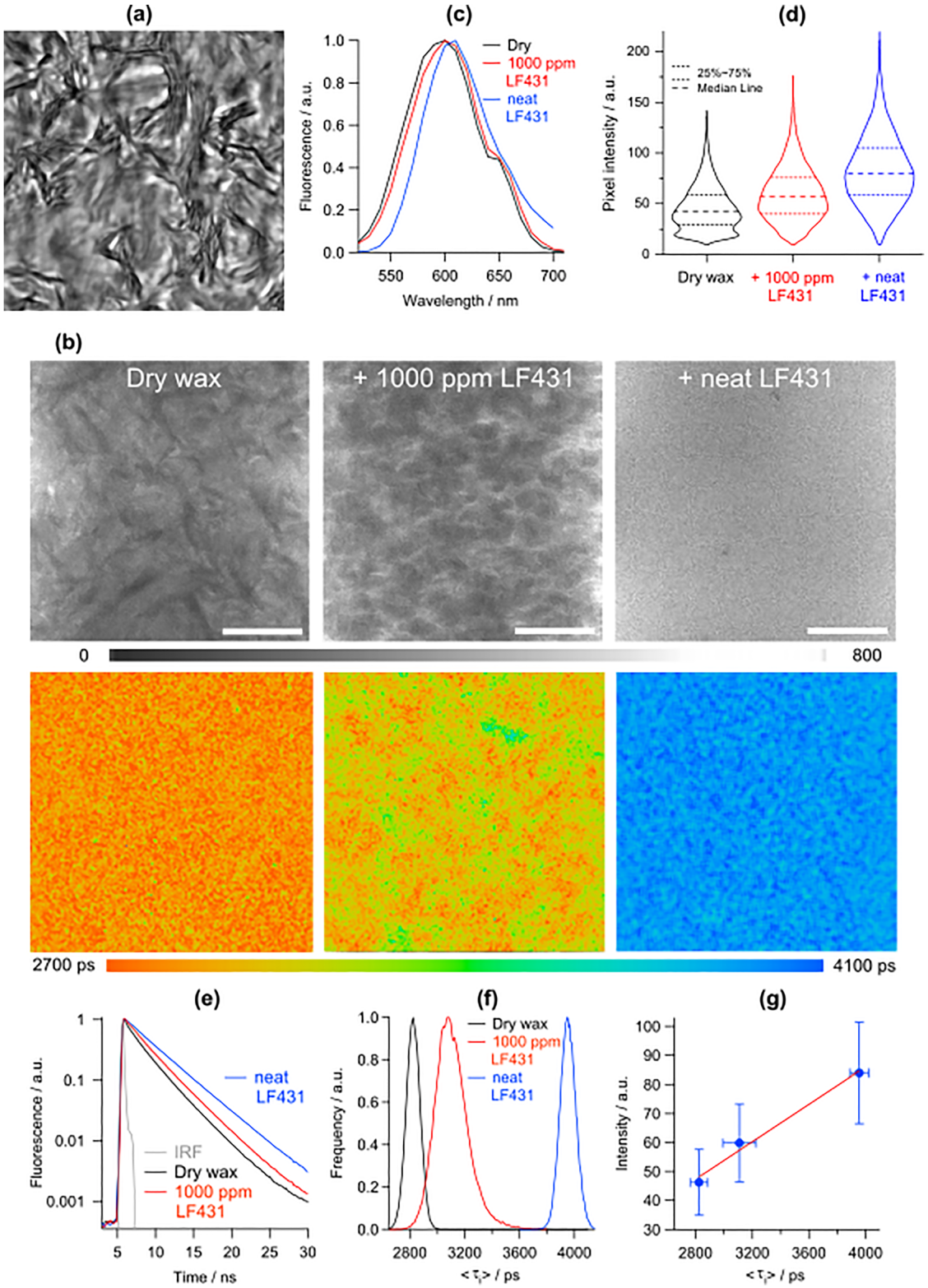

Fig. 3 (a) Transmission, (b) fluorescence intensity (upper row) and FLIM (bottom row) images of Carnauba Wax samples stained with 330 ppm of **Nile Red**: the three columns correspond to dry wax, wax exposed for 60 min to aqueous solution of 1000 ppm of Plurafac® LF431 and wax exposed to the neat Plurafac® LF431, respectively. (c) Normalised fluorescence spectra and (d) intensity distributions in raw confocal images. (e) Fluorescence decay traces and (f) τ_i histograms obtained from samples presented in (d). (g) The averaged intensities per frame (N = 6 for each condition) *vs.* averaged lifetimes obtained from (f); the line is given as a visual guide. All data were obtained after excitation at 930 nm and detection at 540–700 nm. Scale bars are 20 μm.

samples were additionally kept overnight in the desiccator to remove possible residual traces of solvents used. No changes in lifetimes between samples prepared with chloroform and toluene (Fig. S5) illustrated no impact of hydrochloric acid. Overnight degassing of wax samples in the desiccator resulted in a small increase in lifetime for both solvent preparations, which we tentatively attribute to more pronounced phase separation within the wax at these conditions. Due to the minor effects of desiccation on NR lifetimes, all wax samples were prepared under standard conditions without incubation in the desiccator.

The exposure of wax to the adjuvant Plurafac® LF431, both as an aqueous solution (1000 ppm) and the neat compound, results in a significant increase of both the intensity (Fig. 3d) and the τ_i values (Fig. 3e and f) with a good linear correlation between the two parameters (Fig. 3g). In the case of an aqueous solution of LF431, the appearance of bright net-like structures correlates well with positions of pixels with high τ_i values (Fig. 3b, middle column). However, our co-staining experiments with crystalline phase-located molecular rotor (B6++), show minor overlap with NR, either before or after exposure to LF431 (Fig. 2(a3–c3)). Hence, we confirmed that the bright needle-like structures that appeared after the adjuvant penetration (Fig. 1) correspond to the adjuvant-infused amorphous phase of the wax.

In the case of the wax treated with the neat adjuvant, NR exhibits monoexponential decays and even distributions of both intensity and τ_i (Fig. 3e, d and f), without any bright or needle-like features being observed (Fig. 3b, right column). However, the staining with B6++ still shows needle-like structures characteristic of the crystalline phase, even in the case of neat LF431 treatment (Fig. 2a4–c4). Therefore, the concentrated LF431 treatment does not affect the crystalline phase; however, it completely transforms (possibly dissolves) the amorphous wax phase. Monoexponential decays (Fig. 3e) indicate that neat LF431 treatment results in a complete dissolution of NR and formation of a homogenous environment around the dye, consistent with our previous molecular rotor-based study.[9] Additionally, NR lifetime histograms show narrow τ_i distributions for the dry wax and the wax exposed to neat LF431 (Fig. 3f). A broader τ_i distribution for the wax exposed to the aqueous solution of adjuvant was observed, which indicates a larger variety of NR microenvironments formed in response to the aqueous adjuvant penetration.

Thus, the adjuvant penetration induces only a slight increase in the polarity within the wax. However, under these conditions, NR exhibits a remarkable increase in the τ_i values (Fig. 3f), which correlates with the significant increase in NR intensity (Fig. 1 and 3g). This lifetime increase is puzzling and warrants further investigation.

NR emission in bulk solvents

Carnauba wax is a low-polar medium with a dielectric constant ε = 2.5 at 20 °C.[4] Previous studies have shown that in bulk solvents with a broad range of polarities, ε = 2.4–37, NR exhibits fluorescence lifetimes (τ) around 4.0–4.5 ns,[11–14] which are significantly longer as compared to the $\tau_i \approx$ 2.8 ns observed for untreated samples of Carnauba wax (Fig. 3f). However, the τ_i values reached 4.0 ns after the addition of the neat adjuvant to the wax. Therefore, a lower τ_i value seen for NR within the untreated wax as compared to bulk solutions of low polarity must originate from quenching of NR emission, either *via* photochemical reactions with wax components, or through environmental parameters induced by wax components.

We already excluded high polarity as one such factor based on minor shifts observed in the emission spectra, Fig. 3. Other possible parameters include (i) very low polarity, *e.g.* NR dissolved in non-polar solvents such as cyclohexane ε = 2.02 was previously shown to display low lifetime of 2.8 ns;[13] (ii) protic environments can induce quenching, *e.g.* solvents such as alcohols (methanol, ethanol) and water.[11,13,14] Carnauba wax is a complex medium, composed of long alkyl esters of which 40% are ω-hydroxy acid esters, diesters of cinnamic acid and alcohols.[2–4] The intramolecular hydrogen bonds between ω-hydroxy acid esters were suggested to be responsible for the formation of the crystalline phase within the wax.[4] Considering the relatively high heterogeneity of Carnauba wax's composition, one can assume that NR is in domains of ultralow polarity or, alternatively, in proximity to hydrogen-bond donating wax components. To verify this hypothesis, we used bulk solvents of (i) ultra-low polarity (binary mixtures of *n*-pentane, ε = 1.85, and chloroform, ε = 4.81) and (ii) low polar solvent (toluene) with the addition of small quantities of hydrogen bond-rich solvent (methanol, MeOH). However, NR's lifetime remained high around 4 ns for the polarity variation in the range of ε = 2.0 – 4.8 and the presence of up to 10% of MeOH in toluene (v/v); see full datasets in Fig. S6 of SI. These results show that bulk solvents of variable polarity and hydrogen bonding are unable to reproduce the photophysical behaviour of NR within lipid-rich media, such as plant wax.

Recently, we demonstrated that adjuvant penetration significantly reduces the viscosity of amorphous wax.[9] To verify the role of viscosity in observed changes in τ_i values, we measured NR lifetimes within low polarity solutions of different viscosities, *i.e.* toluene/castor oil binary mixtures of different compositions. Our results showed that the emission maxima and lifetimes (app. 3.75 ns) of NR are viscosity independent for a broad range of viscosities (0.5–920 cP); see full datasets in Fig. S6 of SI. Therefore, viscosity can be ruled out as the environmental parameter affecting NR lifetime.

To verify the assumption of NR emission quenching by Carnauba wax components, we recorded NR emission spectra and decay traces of NR in chloroform in the presence of different wax concentrations, see Fig. S7 (SI) for full datasets. The increase in wax concentration results in minor changes in the emission spectra and in a monotonic decrease in lifetime (Fig. S7) that directly confirms the quenching of NR emission by some of the wax components.

The impact of wax structure on NR emission quenching

Since we confirmed the Stern–Volmer quenching of NR by wax components, we next investigated whether the wax structure has any impact on the NR lifetime. Hence, we prepared two

Carnauba wax samples with different morphologies, featuring co-existing crystalline and amorphous phases, which could be obtained by slow and fast cooling of the melted wax.[25] The fast-cooled sample exhibits a noticeable reduction in the size of needle-like structures, suggesting a decrease in size and/or the percentage of crystalline domains. We also observed elevated τ_i values for NR in fast-cooled wax samples, as compared to the slow-cooled wax (Fig. S8). Thus, a fast-cooled sample shows a decrease in the quenching efficiency, even though it has the same chemical composition overall.

Additionally, we carried out experiments with Candelilla wax, an epicuticular wax extracted from the leaves of the Candelilla shrub (*Euphorbia antisyphilitica*). The compositions of two waxes are known to differ, with Candelilla wax typically having a higher hydrocarbon content.[2] The difference in composition leads to differences in morphologies of amorphous and crystalline phases in Candelilla wax, revealed by fluorescence imaging (Fig. 4a–c). However, NR still stains the amorphous phase of Candelilla wax, as shown by the lack of co-staining with B6++ (Fig. 4a–c). NR exhibits an emission at 590 nm, which is slightly blue shifted compared to Carnauba and significantly longer lifetimes of NR were detected, around 3.35 ns (Fig. 4). This indicates that Candelilla wax is still a medium of low polarity (even somewhat lower than Carnauba) and has lower amounts and/or different localisation of wax components that can quench NR emission. Exposing Candelilla wax to neat LF431 results in an increase of NR lifetime (Fig. 4) that confirms that the adjuvant has a similar effect on amorphous phases of both waxes, despite their different composition and morphology.

Previously, NR and its derivatives were extensively studied in lipid bilayers,[15–18] where lifetimes in the range 3–5 ns were observed, depending on the composition of lipid model systems. The general trend was an increase of lifetime with the increase of lipid ordering, *e.g.* bilayers formed from unsaturated lipids (so-called liquid-disordered phase, L_d) showed lower lifetimes, 3.6–3.9 ns, while bilayers formed from saturated lipids and cholesterol (so-called liquid ordered phase, L_o)[15–18] showed larger lifetimes, reaching the value of 7.4 ns in lipid compositions rich in cholesterol.[18] We note that the trend observed in plant waxes is opposite, where adjuvant-induced softening of waxes (*i.e.* a decrease in the ordering of medium) increased NR lifetime. This discrepancy additionally confirms the quenching of NR emission by some of waxes' components.

Given that both Carnauba and Candelilla waxes consist of long aliphatic chain acids with various degrees of saturation,[2,3] which are structurally similar to lipids, we compared NR emission from wax samples with dry lipid mixtures of various compositions. We verified that the observed quenching of NR emission could be observed in dried lipid samples, Fig. S9 and S10. The lifetimes of NR ranged between 3.4–3.6 ns in single-component DSPC, Sphingomyelin and cholesterol samples, and the NR lifetime was further lowered in the samples produced from binary mixtures of Cholesterol/Sphingomyelin and Cholesterol/DSPC, 1/1 (w/w).

Dried lipids and their mixtures form various polymorphs, which could be distinguished by different morphologies of structures formed on the coverslip and observed by transmission imaging (Fig. S9). NR within lipid polymorphs with a clear

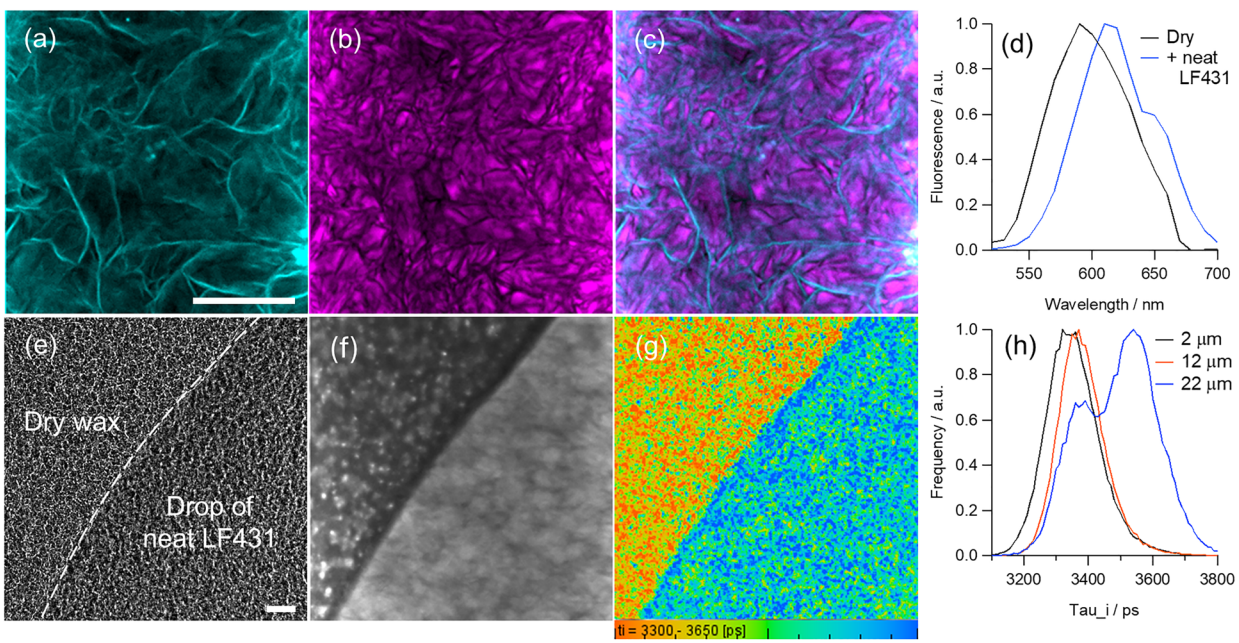

Fig. 4 (a–c) Fluorescence intensity images recorded with dry Candelilla Wax sample co-stained with 100 ppm of B6++ and 30 ppm of **Nile Red**, visualising the (a) crystalline and (b) amorphous phases, respectively; (c) merged images. (e) Transmission, (f) fluorescence intensity and (g) FLIM images recorded with Candelilla wax sample stained with a drop of neat LF431. Dash curve in (e) visualises the edge of adjuvant drop onto the wax surface. The excitation at 930 nm and detection in the range of 480–530 nm for B6++ (a) and 600-700 nm for NR (b and f). (d) Fluorescence spectra and (h) τ_i histograms obtained with sample presented in (e and g). Scale bars are 20 µm.

needle-like patterns demonstrated the lowest lifetime values of 3.0–3.2 ns (Fig. S9 and S10), which were close to τ_i values obtained for untreated Carnauba wax (Fig. 3f). Considering the known fact that cholesterol does not quench NR emission in lipid bilayers,[15,18] this clearly demonstrates the impact of polymorph structure on the efficiency of NR lifetime quenching (Fig. S9–2).

Therefore, the observed quenching of NR emission is a general feature of a lipid-like environment (Fig. 3 and Fig. S9). Our microscopy experiments showed that NR demonstrated very low photobleaching in two waxes (Carnauba and Candelilla) and in dried lipid films under prolonged exposure to intense laser radiation. Therefore, we can assume that this quenching is physical (energy dissipation) rather than photochemical in nature.

Visualisation of adjuvant propagation within the wax

Based on our data, NR provides a unique opportunity to visualise the migration of agriculturally relevant formulations within the amorphous phase of plant wax, as long as adjuvants (such as LF431) alleviate the wax-induced quenching. To clarify the general applicability of this approach, the sensitivity of NR to the penetration of pure water and two commonly used agrochemicals, we recorded four parallel datasets: (i) dry wax, (ii) wax exposed to water and waxes exposed to aqueous solutions of 1000 ppm of (iii) emulsifier (Agnique® CSO40) and (iv) adjuvant (Plurafac® LF431). Agnique® CSO-40 is a non-ionic emulsifier used to stabilise formulations, which is thought to have no impact on the viscosity within both crystalline and amorphous phases of wax.[9] As mentioned before, the Plurafac® LF431 is a softening adjuvant, which mainly affects the amorphous phase of wax.[9] All wax samples were exposed to aqueous solutions of chemicals simultaneously in our custom-designed chamber.[9]

Spectral and FLIM datasets for NR were obtained at different time intervals after exposure to aqueous solutions. Fig. 5a shows FLIM images of all samples after 48 hours of the experiment, and Fig. 5b illustrates the adjuvant-induced changes in NR lifetime within the wax seven hours after the exposure. This data was recorded at different z positions within the wax to assess the spatio-temporal effect of solutions placed on top of the wax layer; the position of the *z*-axis relative to the wax and a glass coverslip is given in Fig. 5c. The expanded datasets, fluorescence intensity and FLIM images are given in Fig. S11 and the emission spectra in Fig. S12, respectively. Fluorescence emission spectra of samples and *z*-profiles of changes to NR lifetimes under four different conditions are displayed in Fig. 5d and e, respectively.

Our spectral data shows a very minor impact of both water and emulsifier/adjuvant on the position of the NR emission maximum (Fig. 5d). The analysis of spectral data was also performed with the Generalised Polarisation (GP) approach, often used to quantify changes in polarity within cellular plasma membranes using charge-transfer dyes (such as Laurdan).[26] Considering the wax environment as similar to lipids, GP analysis could be useful to highlight trends in polarity and fluidity changes. Details on GP calculations with NR are given in SI. *Z*-Profiles of GP values (Fig. S12e) have shown only small changes in wax polarity with two trends visible: (i) an increase in polarity going from the bottom to the top of the wax layer and (ii) an increase in polarity upon exposure to aqueous solutions, with no sensitivity to emulsifier and adjuvant. This change seems reasonable considering the penetration of water from atmospheric air and aqueous solution from the wax layer's top. This can also be correlated with the decrease in rigidity in the same direction, previously revealed with molecular rotors for both amorphous and crystalline phases of the wax.[9]

At the same time, NR shows unusual and unexpected trends in lifetime data upon adjuvant penetration, namely a large increase in τ_i, which does not correlate with polarity (Fig. 5e). The reason for this trend is that polarity changes are very small and their effect on NR can be ignored, compared to a large effect caused by the reduction in quenching, alleviated by the adjuvant (Fig. 3).

The lifetime data demonstrate that NR is primarily sensitive to the penetration of adjuvant, and its propagation within the wax could be clearly visualised by the corresponding *z*-profiles of lifetime (Fig. 5e). While the dynamics of the lifetime increase depends on the thickness of the wax layer (*e.g.* compare the data from three repeats, Fig. 1, 3 and 5), the trend of significant impact of the adjuvant on the amorphous phase is clear to see. The complete saturation of wax with Plurafac® LF431 can be seen at later times in the experiment (filled red circles, Fig. 5e). The observed τ_i values for the aqueous solution of Plurafac® LF431 are lower as compared with the neat adjuvant (Fig. 3f) that should be related to different ratios of wax/adjuvant in these samples, reducing the alleviation effect from the quenching. There was no change in lifetime corresponding to the penetration of pure water or an emulsifier Agnique® CSO40, indicating no disruption of wax-induced quenching of NR emission by water and emulsifier (Fig. 5e).

Mechanism of adjuvant-induced changes in NR emission

To clarify the mechanism behind the increase in NR lifetime upon adjuvant penetration into wax, we tested NR emission spectra and lifetimes in aqueous solutions in the absence and presence of 1000 ppm of Plurafac® LF431, see Fig. 6a and b. In a pure aqueous solution, NR exhibits weak fluorescence and a short lifetime (τ = 0.5 ns). A very weak and redshifted emission maximum (660 nm), together with a partial dye's precipitation within minutes of mixing, indicates significant dye aggregation. Upon the addition of adjuvant, the emission intensity and lifetime increase significantly (τ_i = 3.8 ns), the emission maximum blue-shifts to 640 nm with no evidence of NR precipitation. We hypothesised that this behaviour is caused by the inclusion of NR into the micelles formed by hydrophobic LF431 (the Critical Micellar Concentration, CMC, of 4.2 mg L^{-1} or 4.2 ppm; unpublished data measured at BASF).

Next, we recorded the same data for NR in the neat adjuvant. Further blueshift of the emission maximum is seen to 610 nm with an increase in lifetime up to 3.9 ns (Fig. 6a and b). These

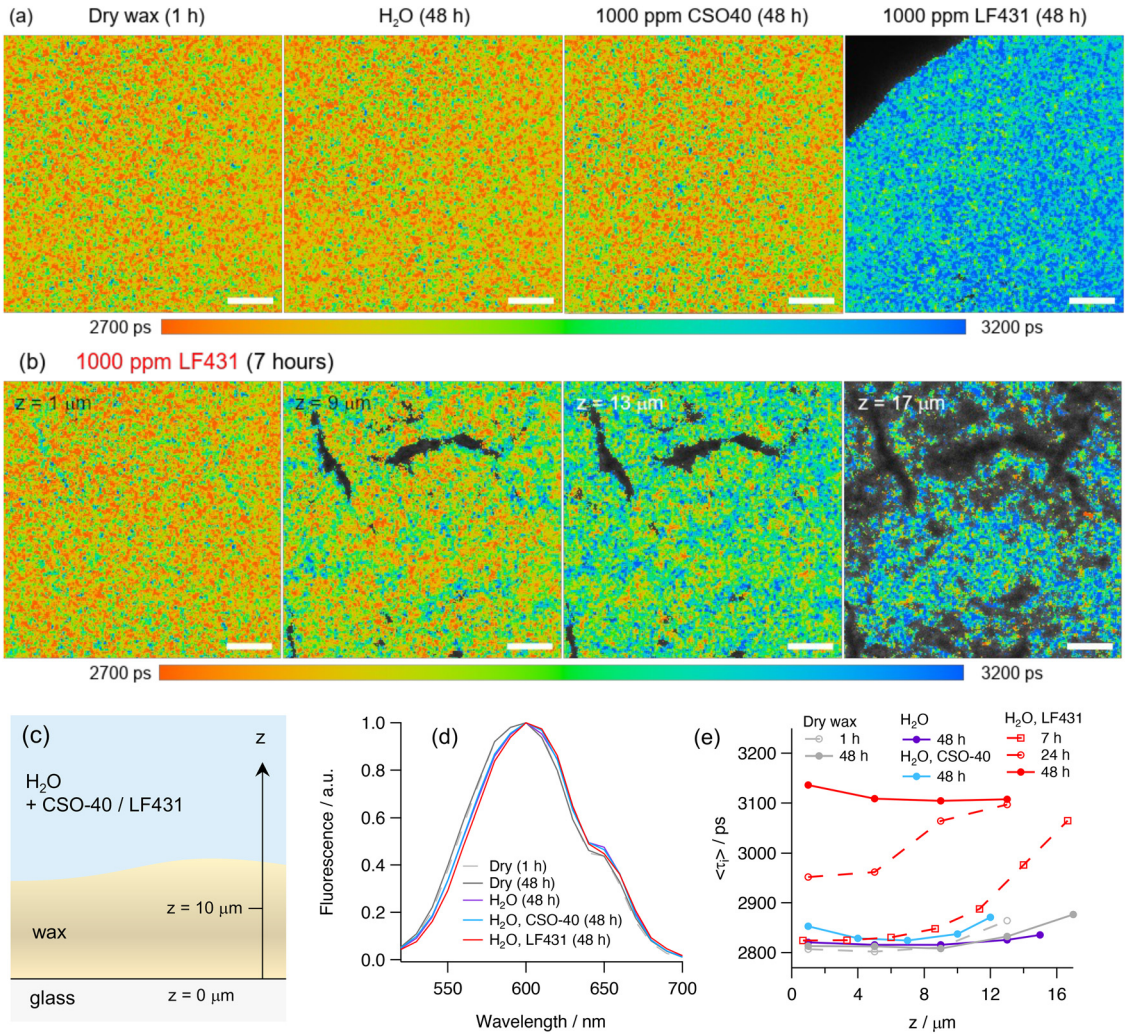

Fig. 5 FLIM data for Carnauba wax samples stained with 330 ppm NR under four different conditions: (i) dry wax and the wax stained with (ii) pure water in the absence and presence of 1000 ppm of (iii) emulsifier Agnique® CSO40 or (iv) adjuvant Plurafac® LF431 at different time intervals. (a) dry wax; (b) 1000 ppm aqueous solution of adjuvant Plurafac® LF431 after 7 hours of exposure. Images were recorded with the excitation at 930 nm and emission detection at 520–700 nm. The scale bar for all images is 40 μm; the full set of images can be found in SI, Fig. S7. (c) Schematic representation of the wax exposure to aqueous solutions containing the emulsifier or the adjuvant (taken from ref. 9); all images are given for the lowest positions within the wax, $z \approx 1$–2 μm. (d) Fluorescence emission spectra of samples obtained with the excitation at 930 nm. (e) z-Profiles of t_i values for NR within waxes stained under various conditions as indicated in the figure legend on the right.

parameters are close to those seen for NR in chloroform. The similarity in the lifetimes recorded for NR in neat adjuvant (3.9 ns) and within the wax stained with the neat adjuvant (4.0 ns, Fig. 3f) indicates that NR is likely completely dissolved and protected from the wax component quenching under these conditions. It should be noted that the τ_i values of 3.1 ns for NR within the wax stained with the aqueous solution of LF431 (Fig. 3f and 5e) are significantly shorter as compared to the τ_i = 4.0 ns, recorded in the presence of the neat adjuvant (Fig. 3f). It seems likely that LF431 provides only a partial protection from wax quenching under the dilute conditions of aqueous solution (which are also agriculturally relevant). However, the lifetime signatures of NR can clearly visualise the penetration of LF431 inside the wax, even as an aqueous solution, which presumably coincides with the penetration of a desired agrochemical. (Fig. 1 and 3b–d).

As a control, we measured the spectra and lifetime of NR in an aqueous solution and the presence of 1000 ppm of emulsifier Agnique® CSO40 and recorded spectra and lifetimes that closely match those recorded with adjuvant LF431 (τ = 4.2 ns) (Fig. 6c and d). This data indicates that NR prefers a hydrophobic micellar environment created by CSO40 (CMC 180 mg L^{-1}) to an aqueous environment where it dissolves poorly. However, no change in the wax lifetime of NR (the presence of CSO40, Fig. 5e) is consistent with no penetration of CSO40 inside wax.[9]

To verify that the visualisation of softening adjuvant's propagation inside the plant wax is a general feature of NR, we recorded a set of data with three other adjuvants, Plurafac® LF1300, Agnique® SBO10 and Lutensol® XP80, which are characteristic representatives of different classes of softening adjuvants available commercially (CMCs are 50, 90 and 540 mg L^{-1}). First, the spectral

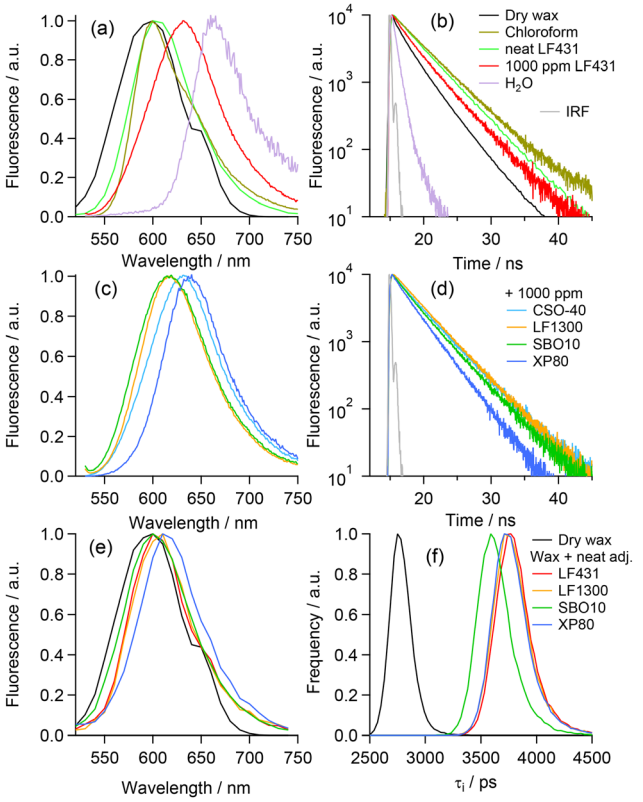

Fig. 6 (a) and (c) NR emission spectra and (b) and (d) fluorescence decay traces recorded after the excitation at 467 nm and the detection at the emission maxima for corresponding media. (a) and (b) NR in the aqueous solution in the absence (violet) and presence of 1000 ppm of Plurafac® LF431 (red), the neat Plurafac® LF431 (green) and chloroform (gold). Data for NR in the dry Carnauba wax (black) are given for comparison. (c) and (d) NR in the aqueous solution in the presence of 1000 ppm of the emulsifier Agnique® CSO40 (light blue) and softening adjuvants Plurafac® LF1300 (orange), Agnique® SBO10 (green) and Lutensol® XP80 (dark blue). (e) Fluorescence emission spectra and (f) distributions of τ_i values for Carnauba wax samples stained with 330 ppm NR and exposed to the neat adjuvants (the same colours).

and lifetime data for NR in aqueous solutions with the presence of 1000 ppm of each adjuvant were recorded (Fig. 6c and d and Fig. S13). All the data points towards encapsulation of NR in micelles made up of these hydrophobic adjuvants, resulting in high brightness with blue-shifted emission and long lifetimes of NR. Next, we imaged NR-stained Carnauba wax samples exposed to the neat adjuvants (Fig. 6e and f and Fig. S14–S16). The penetration of neat adjuvants induces small red shifts in the emission spectra (Fig. 6e and Fig. S15) and a remarkable increase in lifetime, similar to that seen with Plurafac® LF431 (Fig. 6e and Fig. S16). Our data clearly demonstrates that NR's quenching by the wax components makes it a useful sensor for the penetration of wax by hydrophobic agrochemicals, seen as a reduction in its quenching.

NR *vs.* molecular rotors for visualisation of adjuvant penetration

Results of this and our previous work[9] show that both NR and molecular rotors could visualise the adjuvant penetration into the amorphous phase of the plant waxes. The use of molecular rotors is beneficial for quantifying changes in viscosity using a lifetime-based approach, as measured lifetimes could be directly converted to viscosities using a calibration curve.[9] The quantification of changes with NR is less straightforward because the degree of change depends on several conditions, such as the distribution of wax components that can quench the NR emission and the initial dye concentration that may lead to lifetime quenching (Fig. S4). However, NR can easily visualise adjuvant penetration *via* a large increase in its fluorescence intensity (Fig. 1). The aggregation of NR within wax at high NR concentrations is not an obstacle for intensity-based quantification, since adjuvant alleviates both self- and wax-mediated quenching effects. At the same time, the intensity of molecular rotors decreases upon adjuvant penetration.[9] Qualitative measurements of viscosity with molecular rotors offer unique and concentration-independent insight, but they require access to FLIM, while quantitative assessments with NR could be done using any microscope (confocal or widefield) with fluorescence detection. Thus, NR could find its application in agrochemical research as a cheap, commercially available and easy-to-use tool.

Conclusions

Our results show that the environmentally sensitive fluorophore, **Nile Red** (NR), readily incorporates into two types of plant waxes (Carnauba and Candelilla) and dry lipid films composed of both individual lipids and lipid mixtures. Confocal and fluorescence lifetime imaging (FLIM) microscopy studies demonstrated that NR fluorescence is significantly quenched within the above structures, which was not reported previously, even though NR is a common lipid environment probe.

Our control experiments were able to assign the quenching to physical excited-state deactivation processes within wax, which are microstructure- and concentration-dependent. Interestingly, the quenching can be alleviated by the administration of adjuvants, hydrophobic agrochemicals which are routinely included in pesticide formulations and known to soften the wax. The protection of NR from wax quenching offered by adjuvants provides a unique opportunity for NR to be used to visualise the permeation of agrochemicals in plant waxes using conventional confocal microscopes by an increase in brightness of the dye's fluorescence.

Author contributions

P. S. S. and M. W. C. L.: data acquisition and analysis, P. S. S.: writing of the first manuscript draft; N. J. B: equipment; M. R.: conceptualisation, funding; M. K. K.: equipment and resources, overall project supervision. The manuscript was co-edited and co-written by all authors.

Conflicts of interest

Adjuvants used in this work (Plurafac® LF431, Plurafac® LF1300, Agnique® SBO10, Lutensol® XP80) and the emulsifier

(Agnique® CSO40) are sold by the company associated with this study (BASF).

Data availability

The data supporting this article have been included as part of the supplementary information (SI).

The following datasets are available to researchers upon request to the authors:

- Absorption and fluorescence spectra recorded by Agilent UV-vis DataStation spectrophotometer (Agilent HP 8453, *.sd) and Horiba FluoroMax 4 spectrofluorometer (Jobin-Yvon, Horiba, *.opj);
- Time-Correlated Single Photon Counting (TCSPC) data files generated by Horiba's DataStation Software (*.das);
- Confocal and multiphoton images and emission spectra in Leica Image Format (*.lif);
- Fluorescence Lifetime Imaging Microscopy (FLIM) datasets in Beckl&Hickl formats as raw (*.sdt) and analysed data files (*.img);
- Summarised emission spectra and fluorescence decay traces plotted in IgorPro v.6.2 (*.pxp).

Supplementary information is available. See DOI: https://doi.org/10.1039/d5tb02086g.

Acknowledgements

We thank our BASF colleagues from the Industrial Formulators, Doris Kremzow and Ingo Fleute-Schlachter, for their support and Sven Janson for conducting experiments at BASF. MKK is grateful to the EPSRC for a Career Acceleration Fellowship (EP/I003983/1).

References

1 T. H. Yeats and J. K. C. Rose, *Plant Physiol.*, 2013, **163**, 5–20, DOI: 10.1104/pp.113.222737.
2 E. Krendlinger, U. Wolfmeier, H. Schmidt, F.-L. Heinrichs, G. Michalczyk, W. Payer, W. Dietsche, K. Boehlke, G. Hohner and J. Wildgruber, Waxes, *Ullmann's Encyclopedia of Industrial Chemistry*, 2015, DOI: 10.1002/14356007.a28_103.pub2.
3 L. S. Devi, S. Kalita, A. Mukherjee and S. Kumar, *Trends Food Sci. Tech*, 2022, **129**, 296–305, DOI: 10.1016/j.tifs.2022.09.019.
4 T. D. Callinan and A. M. Parks, *1959 Conference on Electrical Insulation*, 1959, pp. 45–49, DOI: 10.1109/EIC.1959.7533355.
5 I. Basson and E. C. Reynhardt, *J. Phys. D: Appl. Phys.*, 1988, **21**, 1429–1433, DOI: 10.1088/0022-3727/21/9/017.
6 S. Merk, A. Blume and M. Riederer, *Planta*, 1997, **204**, 44–53, DOI: 10.1007/s004250050228.
7 Y. Zhang, M. J. Adams, Z. Zhang, O. Vidoni, B. H. Leuenberger and J. Achkar, *Polymer*, 2016, **86**, 208–219, DOI: 10.1016/j.polymer.2016.01.033.
8 S. Brychka, A. Brychka, N. Hedin and M. Mondeshki, *Materials*, 2024, **17**, 1978, DOI: 10.3390/ma17091978.
9 P. S. Sherin, M. Rueckel and M. K. Kuimova, *Chem. Biomed. Imaging*, 2024, **2**, 453–461, DOI: 10.1021/cbmi.4c00005.
10 P. Greenspan, E. P. Mayer and S. D. Fowler, *J. Cell Biol.*, 1985, **100**, 965–973, DOI: 10.1083/jcb.100.3.965.
11 G. B. Dutt, S. Doraiswamy, N. Periasamy and B. Venkataraman, *J. Chem. Phys.*, 1990, **93**, 8498–8513, DOI: 10.1063/1.459288.
12 A. K. Dutta, K. Kamada and K. Ohta, *J. Photochem. Photobiol., A*, 1996, **93**, 57–64, DOI: 10.1016/1010-6030(95)04140-0.
13 A. Cser, K. Nagy and L. Biczók, *Chem. Phys. Lett.*, 2002, **360**, 473–478, DOI: 10.1016/S0009-2614(02)00784-4.
14 J. A. Levitt, P.-H. Chung and K. Suhling, *J. Biomed. Opt.*, 2015, **20**, 096002, DOI: 10.1117/1.JBO.20.9.096002.
15 S. Mukherjee, H. Raghuraman and A. Chattopadhyay, *Biochim. Biophys. Acta*, 2007, **1768**, 59–66, DOI: 10.1016/j.bbamem.2006.07.010.
16 F. Ragaller, L. Andronico, J. Sykora, W. Kulig, T. Rog, Y. B. Urem, Abhinav, D. I. Danylchuk, M. Hof, A. Klymchenko, M. Amaro, I. Vattulainen and E. Sezgin, *Open Biol.*, 2022, **12**, 220175, DOI: 10.1098/rsob.220175.
17 F. Ragaller, E. Sjule, Y. B. Urem, J. Schlegel, R. El, D. Urbancic, I. Urbancic, H. Blom and E. Sezgin, *J. Phys. Chem. B*, 2024, **128**, 2154–2167, DOI: 10.1021/acs.jpcb.3c07006.
18 R. B. Lira, L. S. Dillingh, J.-J. Schuringa, G. Yahioglu, K. Suhling and W. H. Roos, *Biophys. J.*, 2024, **123**, 1592–1609, DOI: 10.1016/j.bpj.2024.04.033.
19 G. Sancataldo, G. Avellone and V. Vetri, *Environ. Sci.: Processes Impacts*, 2020, **22**, 2266–2275, DOI: 10.1039/d0em00348d.
20 R. Kumar Gautram, A. Bapli, R. Jana and D. Seth, *J. Photochem. Photobiol., A*, 2020, **399**, 112550, DOI: 10.1016/j.jphotochem.2020.112550.
21 M. Alhibah, M. Kröger, S. Schanzer, L. Busch, J. Lademann, I. Beckers, M. C. Meinke and M. E. Darvin, *Pharmaceutics*, 2022, **14**, 1790, DOI: 10.3390/pharmaceutics14091790.
22 M. K. Kuimova, G. Yahioglu, J. A. Levitt and K. Suhling, *J. Am. Chem. Soc.*, 2008, **130**, 6672–6673, DOI: 10.1021/ja800570d.
23 I. López-Duarte, T. T. Vu, M. A. Izquierdo, J. A. Bull and M. K. Kuimova, *Chem. Commun.*, 2014, **50**, 5282–5284, DOI: 10.1039/c3cc47530a.
24 W. Becker, *The BH TCSPC Handbook*, 8th edn, 2019, p. 783. https://www.becker-hickl.com/literature/documents/flim/the-bh-tcspc-handbook/.
25 A. I. Blake, E. D. Co and A. G. Marangoni, *J. Am. Oil Chem. Soc.*, 2014, **91**, 885–903, DOI: 10.1007/s11746-014-2435-0.
26 W. Yu, P. T. So, T. French and E. Gratton, *Biophys. J.*, 1996, **70**, 626–636, DOI: 10.1016/S0006-3495(96)79646-7.

